TIME-DEPENDENT DESCRIPTION OF CLUSTER FORMATION

Z. Basrak[1,2], P. Eudes[2], P. Abgrall[2], F. Haddad[2], and F. Sébille[2]

[1] *Ruđer Bošković Institute, HR-10 001 Zagreb, Croatia*
[2] *Laboratoire SUBATECH, Université de Nantes, École des Mines de Nantes, IN2P3/CNRS, F-44 072 Nantes Cedex 03, France*

A model allowing to simulate the production of clusters at each step of the reaction is developed and applied to heavy-ion collisions at intermediate energies. The collision process is entirely governed by the Landau-Vlasov model which provides the time evolution of the one-body phase-space distribution. Particles emitted during successive time intervals of the dynamics are gathered together into subensembles to which a percolationlike procedure is applied. Comparison with the experimental data for the Ar(65 MeV/nucleon) + Al reaction shows that the average behavior of particle dependent global observables is correctly reproduced within this framework. These results point out that studied global properties of heavy ion collisions greatly rely on the out-of-equilibrium behavior of the nuclear dynamics. The adopted approach takes into account the spreading of the wave packets associated with each emitted nucleon.

PACS numbers: 24.10.-i, 24.90.+d, 25.70.-z, 25.70.Gh

I. INTRODUCTION

Heavy-ion induced reactions at intermediate incident energies are characterized by an abundant production of intermediate mass fragments and light charged particles whose variety increases with energy of the projectile and mass of the colliding nuclei. It is generally admitted that most of these particles and fragments arise from highly excited nuclear matter. The analysis of experimental data in terms of global observables, such as rapidity, transverse momenta and azimuthal

distributions..., has shown their dependence on the mass of the considered cluster. This dependence may contain valuable informations on nuclear matter properties as well as on the dynamics of the underlying processes. In addition, this mass dependence appears as a powerful tool for probing the different stages of the reaction dynamics. Therefore, it is of interest to theoretically investigate the trends of experimental data observed at intermediate energies.

Several models based on static treatments of nuclear reactions have been elaborated in order to study the cluster formation: an extended version of the evaporation model [1], statistical models (simultaneous or sequential) treating the nuclear system under consideration either as a canonical or a microcanonical ensemble [2–7], and percolation models [8,9]. Models based on percolation formalisms have been extensively used to investigate various nuclear phenomena, such as nuclear matter phase transition and multifragmentation [10–16]. These models rather well reproduce experimental inclusive data like charge or mass distributions [12–16]. Nevertheless, their main drawback is the lack of dynamical informations on the production mechanisms.

In order to investigate the role of dynamical effects, we address this topic starting from a semiclassical dynamical approach. We use the Landau-Vlasov (LV) model [17], which has shown its good predictive power in reproducing the average behavior of collective observables [18–20]. Also, it has been used several times [14,21] as an input model which provides the bulk initial conditions (spatial density, excitation energy, collective behavior, and their impact parameter dependence) for more phenomenological models specifically dealing with fragment production. Let us recall that the LV model is based on the one-body approach and, therefore, does not contain the complete multiparticle correlations expected to play a role in the production mechanisms of light composites. This fact is, obviously, a source of limitation in comparing theoretical and experimental results.

One way to produce light clusters is, for example, to complement the one-body dynamical model by a percolation-type procedure. The success of such approach is, however, strongly dependent on the emission processes involved in the collision. As a matter of fact, an important parameter is the freeze-out time defined as the moment of the collision at which the system starts to radially expand, cools down and reaches the minimum of its average local density. The freeze-out time is relatively well defined at energies above 100 MeV/nucleon and a percolation procedure can be applied to the final configuration space with some success [22,23]. At energies below 100 MeV/nucleon the dynamical situation is much more complex. The freeze-out time cannot be well defined because of the strong interplay between the nuclear mean field and the residual nucleon-nucleon interactions. This interplay generates a highly inhomogeneous spatial distribution where regions of rather high densities coexist with regions of low densities. As a result, the percolation approach is not directly applicable. Therefore, the clusterization process below 100 MeV/nucleon requires developing of a more suited model which would take into account the particular aspects of the dynamical regime involved in the collision. In the following, we focus on the mean behavior of the global properties of heavy ion reactions. The problem of dispersions of the global observables, around their mean values, is out of the scope of this paper.

The paper is organized as follows. Section II describes the method for light-cluster production. The method takes into account the dynamics of the collision and is based on the percolationlike algorithm. In this section, we also discuss the internal consistency of the model and the quantum-mechanical grounds of the adopted algorithm. The application of the model to collisions of Argon on Aluminum nuclei at 65 MeV/nucleon is presented in Sec. III. Section IV summarizes our results.

II. MODEL FOR THE FORMATION OF LIGHT CLUSTERS

A. Outline of the dynamical model

A semiclassical transport equation, such as the LV equation, uses a mean-field approximation to describe the dynamics of a collision of two heavy ions at energies above 10 MeV/nucleon, where pairing and shell effects are considered to be negligible [24]. The one-body phase-space is described by the distribution function $f(\mathbf{r},\mathbf{p};t)$ and its spatial and temporal evolution is governed by the average nuclear mean field H and residual nucleon-nucleon collisions that act via the collision term I_{coll} of the LV equation:

$$\frac{\partial f}{\partial t} + \{f, H\} = I_{coll}(f). \tag{1}$$

The symbol { , } stands for the Poisson brackets. In the LV dynamical approach [17], the nuclear collisions are calculated by projecting the one-body nuclear phase space onto a continuous basis of thousands of coherent states (CS) $g(\mathbf{r},\mathbf{p})$:

$$f(\mathbf{r},\mathbf{p};t) = W(\mathbf{r},\mathbf{p}) * g(\mathbf{r},\mathbf{p};t). \tag{2}$$

The weight function W gives the occupational probability of CS in the initial conditions and is deduced from a semiclassical calculations of the ground states determined iteratively in a self-consistent way. A large number of CS per nucleon N_g and their spatial spreading are needed to ensure a meaningful mapping of the phase space. The Wigner transform of the ith CS is a Gaussian function:

$$g_i(\mathbf{r},\mathbf{p};t) = \frac{1}{(2\pi\sigma_r\sigma_p)^3} exp(-\frac{(\mathbf{r}-\mathbf{r}_i(t))^2}{2{\sigma_r}^2}) \times exp(-\frac{(\mathbf{p}-\mathbf{p}_i(t))^2}{2{\sigma_p}^2}). \tag{3}$$

The centroids of CS move along semiclassical trajectories with constant spreadings σ_r and σ_p in the $\mathbf{r}$ and $\mathbf{p}$ space, respectively, following Ehrenfest type of equations of motion. The self-consistent nuclear mean field is calculated with the nonlocal effective force due to Gogny [25]. The Gogny interaction reproduces not only the basic static properties of colliding nuclei, namely, the saturation density and the ground-state binding energy, but also many nuclear properties, e.g., the depth of the optical potential [26]. The LV model with the Gogny interaction generates a well-defined mean field with a proper surface dependence and includes the Coulomb interaction that is essential to correctly account for lateral motion at low incident energies. The residual interactions are treated as hard stochastic scattering in accordance with the collision term I_{coll} of Uehling and Uhlenbeck [27]. The collision term takes into account energy and momentum conservation as well as the Pauli exclusion principle. It uses the isospin and energy-dependent free nucleon–nucleon cross section σ_{nn} which enters into the collision term I_{coll}.

The nuclear mean field alone is able to stick together CS in heavy remnants. In other words, for densities not too far from the nuclear saturation density, the mean-field approximation is fully justified, but it is not so for the emitted CS, for which the average probability density in coordinate space falls below the one tenth of the initial nuclear density. In this type of semiclassical transport theories, free CS move practically independently of each other. They neither contribute to the nuclear mean field nor feel it. They are just sensitive to the Coulomb interaction. Consequently, without perturbing the dynamics of the collision, one is allowed to consider and treat the population of CS related to emitted particles apart from those that are still bound at any moment.

In the LV approach, the initial phase space is densely mapped. Therefore, in a single simulation shot with fixed initial conditions, a broad final phase space is reached. The time-dependent phase-space distribution of the emission probability is deduced from this one-body distribution by following the trajectories of free CS.

B. Characteristics of the emission process below 100 MeV/nucleon

Successful description of nuclear clusterization, by grafting a percolation method onto a dynamical description of the heavy-ion collision, is strongly dependent on the emission mechanisms involved in the collision. Let us recall briefly why such approaches are very fruitful at energies above 100 MeV/nucleon. At these energies the nucleus-nucleus collisions can be schematically described by the so-called participant-spectator model. In this picture, a highly compressed and heated zone is produced during the early stage of the reaction (a few fm/c). Immediately, it undergoes a decompression leading to a simultaneous formation of light- and medium-mass clusters which radially escape out of the participant zone, all practically *at the same time*, the *freeze-out time*. It is, then, possible to analyze nuclear fragment formation by applying aggregation procedures based on a purely geometrical prescription in configuration or/and in momentum space at the freeze-out time. This procedure can, eventually, be complemented by a deexcitation process in order to describe the sequential evaporation from the excited products.

Two major dynamical characteristics contrast the low energy collisions from the high energy ones: (i) At energies below 100 MeV/nucleon there is no well defined freeze-out time. A colliding system spends a relatively long time (a few tens of fm/c) in an out-of-equilibrium dynamical stage. Before reaching an equilibrated steady state, the nuclear system abundantly emits particles. (ii) The recent experimental studies have shown that reaction mechanism is strongly dominated by dissipative binary collisions [28,29]. The LV calculations are in good agreement with such observed trends [30–33].

The binary feature of the nuclear collision

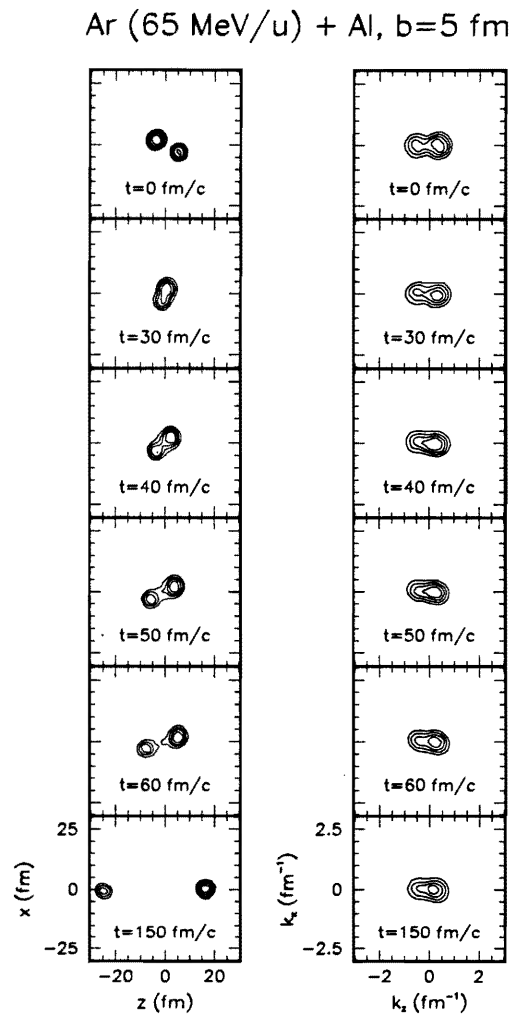

FIG. 1. The time evolution of the equidistant density contours projected onto the reaction plane in the configuration (left) and the momentum space (right). The contours are deduced from the Landau-Vlasov simulation of the Ar + Al collision at 65 MeV/nucleon and an impact parameter of $b = 5$ fm. The $z(k_z)$ axis is along the beam direction.

can be clearly seen in Fig. 1 which depicts a typical heavy-ion reaction below 100 MeV/nucleon: a collision of Argon on Aluminum at 65 MeV/nucleon for an impact parameter of $b = 5$ fm. Figure 1 displays density profiles in the configuration (left side) and momentum space (right side) at several selected times. After nuclei have got in contact, a relatively long-lived binuclear system is formed which undergoes rotation (cf. left side in Fig. 1). At about 25 fm/c, the compression is maximal and the emission rate grows rapidly reaching its maximum at about 60 fm/c as evidenced by the solid curve in Fig. 2. In this first stage of the reaction, particles are emitted from the interaction zone filling up mid-rapidity region. This is illustrated by the upper panel of Fig. 3 where the rapidity distribution of the particles emitted during this time interval is displayed. In this early stage, the two initial overlapping Fermi spheres in the momentum space are rearranged into an elongated pear-shaped configuration which does not evolve with time any further (right side in Fig. 1). An isotropic momentum distribution is achieved locally [34] already at about 30 fm/c (the arrow marked by t_{eq} in Fig. 2), much before a steady global structure is established at 60 fm/c. At that time, a second stage of the reaction begins (left side of Fig. 1 and the arrow marked by t_{sep} in Fig. 2); the two excited equilibrated heavy fragments arise. They are, generally, referred as quasitarget (QT) and quasiprojectile (QP). These heavy remnants of the reaction cool down by emitting particles whose rapidity distribution exhibits maxima located near the target and projectile rapidities, respectively (lower panel in Fig. 3). From the time dependence of the particle emission rate (solid curve in Fig. 2), one sees that a large portion of particles is emitted throughout the first stage of the collision which appears dynamically very complex. Particles emitted at the beginning and at the end of the first stage carry different dynamical fingerprints.

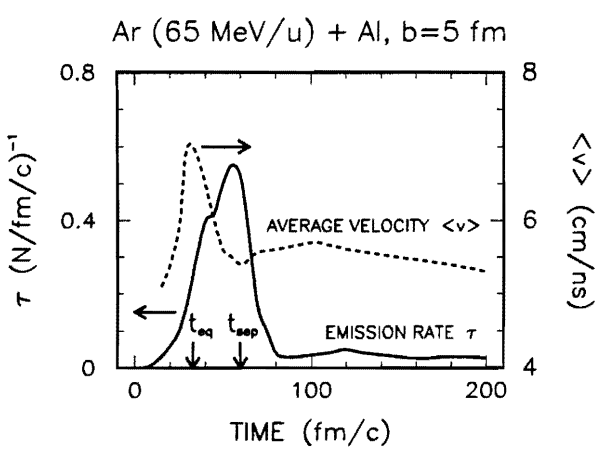

FIG. 2. Number τ of emitted particles per 1 fm/c (full curve and the left-side scale) and the mean speed $\bar{v}$, expressed in cm/ns, of emitted particles with respect to their source of emission (dashed curve and the right-side scale), as a function of time. Calculations are the same as in Fig. 1. For further details, see the text.

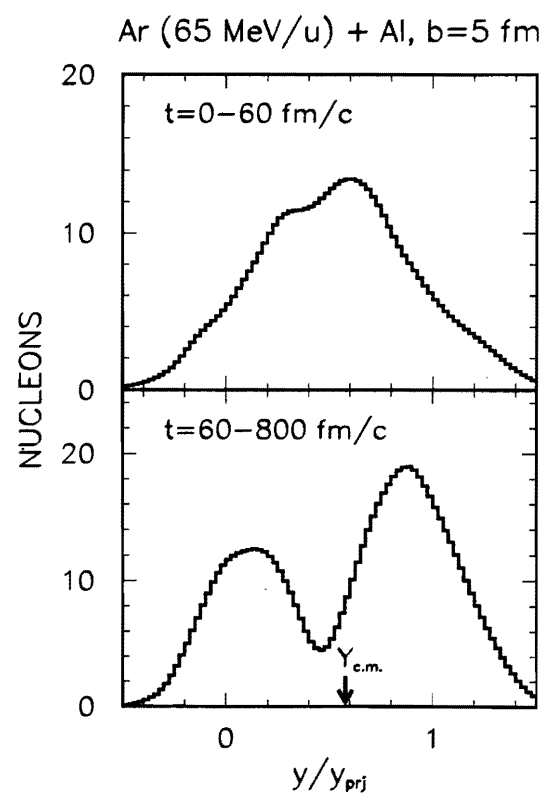

FIG. 3. Distributions of free coherent states (emitted particles) as a function of relative rapidity (the particle rapidity scaled by the projectile rapidity) emitted before (top) and after (bottom) the separation of the quasitarget and the quasiprojectile. Calculations are the same as in Fig. 1. Zero stands at the target rapidity and one at the projectile rapidity. The c.m. rapidity is marked by an arrow labeled $Y_{c.m.}$.

C. Formation of clusters

The main features of the nucleus-nucleus collisions are described within a one-body approach. However, this approach takes into account the correlation effects only implicitly, i.e. through the dissipative nature of the mean behavior. In fact, the multiparticle correlations induce a bundle of phase-space trajectories fluctuating around the mean one. Neither theoretical investigations, nor experimental results currently give access to the full microscopic informations. Hence, the best way to deal with this lack of knowledge is to take a statistical point of view. In this framework the space of the accessible states must be constrained by the fundamental characteristics of the physical process we are addressing. Since different investigations have shown that semiclassical LV model is able to give a satisfactory description of the one-body observables, we will use it to provide us with the ensemble averaged description of the nucleonic distribution. In addition, we are interested in processes occurring in regions of low average density in configuration space. Consequently, a convenient way to span the space of the accessible states is to define each ensemble in terms of an antisymmetrized set of coherent states. The density of this nucleonic distribution is rather low. Within this picture, it means that one can associate a coherent-state wave packet with each nucleon. These coherent states are generalized states [35], and, in principle, their extension in phase space should evolve according to the nuclear interaction they experience. In the following, we are going to treat the discussed general scheme in an approximative way. Essentially, we are aiming to point out whether the topological structure induced by the mean-field dynamics is able, by itself, to provide better understanding of the mass dependence for different observables.

A first attempt in investigating the phase-space topology consists of strictly applying a percolation procedures [8,9]. At projectile energies below 100 MeV/nucleon, the inclusion of this procedure, either at the time when the QP and the QT separate, or at the end of the dynamical calculation gives wrong results. For example, it provides a wrong rapidity dependence of the generated clusters and, moreover, one has to face an overwhelming contribution of neutrons and protons. These large discrepancies result from the fact that one has not taken into account the complex dynamics of the first out-of-equilibrium stage of the collision as well as a distinct emission regime from the QP and the QT that is clearly seen in Figs. 3 and 2, respectively. Obviously, one should not mix particles coming from different dynamical steps of the collision.

In order to restore the influence of the dynamics, we subdivide the ensemble of all CS into parts having the same dynamical history. The CS are gathered together according to their emission time. In this way, we have few subensembles of free CS and a subensemble of those CS which are bound in heavy remnants at the end of the dynamical calculation. Technically, the calculation is carried out in two phases:

i) The definition of subensembles, i.e., of consecutive time intervals of the emission, and evaluation of system properties in a given time interval, such as mean radii R_{FRAG} of emitting heavy fragment(s) and the average speed $\bar{v}$ of emitted CS relative to the emitting heavy fragment.

ii) The application of the cluster-searching algorithm to each subensemble.

An efficient way to generate collision events which have global properties close to those imposed by the one-body distribution, is to randomly sample A nucleons out of the total $(A \times N_g)$ population of CS following an uniform sampling law. The selected set of nucleons (CS) has to be consistent with the conservation laws for mass and charge of target and projectile, respectively. In order to stick to the full phase-space information contained in one-body distribution, the

sampling procedure is refined by adding a random dispersion to the centroids of the position and the momentum of each selected CS. This is done via *Monte Carlo* technique according to the normal distribution whose standard deviation is equal to σ_r and σ_p in the configuration and momentum space, respectively (see Eq. (3)).

For such collision events, an aggregation procedure is applied separately to the nucleons of each subensemble. This procedure is based on a percolation technique. It is restricted to the configuration space in accordance with the work of Campi and Desbois [36]. All nucleons belonging to the subensemble of heavy remnants are bound in their respective heavy fragments. This treatment gives us the QP and the QT of the generated event. To obtain light composites and intermediate mass fragments, a percolation is performed for the rest of nucleons which belong to the population of free CS.

We now sketch how this percolation is performed within each of the above defined subensembles. A sphere of radius R_{PERC}, the *radius of percolation*, is associated with each free nucleon. For each nucleon R_{PERC} is different. Its value is proportional to the distance D_{PERC} of a nucleon from the emitting source (heavy fragment). Determination of R_{PERC} (D_{PERC}) is done in the following way:

i) The distance D_{PERC} to the closest heavy fragment is calculated for each nucleon. The heavy fragment are considered as spheres of radii R_{FRAG} whose values corresponds to the mean-square distances of all bound CS to the heavy fragment center of mass.

ii) The average speed $\bar{v}$ (see the dashed curve in Fig. 2) of all CS belonging to a given subensemble is known from the first preparatory phase of calculation. We require that each nucleon at the heavy fragment surface, i.e., for $D_{PERC} = 0$, has a (constant) *basic radius of percolation* $R^0_{PERC} =$ 0.8 fm. This value is related to the range of the nuclear interaction. Hence, with R_{PERC} ($D_{PERC} = 0$) $= R^0_{PERC}$ and, by assigning the average speed $\bar{v}$ to a free nucleon under consideration, one calculates the opening angle α_{PERC} of a *percolation cone*. This cone envelopes the spheres of radii R_{PERC} and determines linear increase of diameter of these spheres as a function of nucleon distance D_{PERC}. In order to keep as simple as possible the global scheme of the algorithm, we postpone the details of calculating the α_{PERC} to the end of this section (see Eq. (6) below).

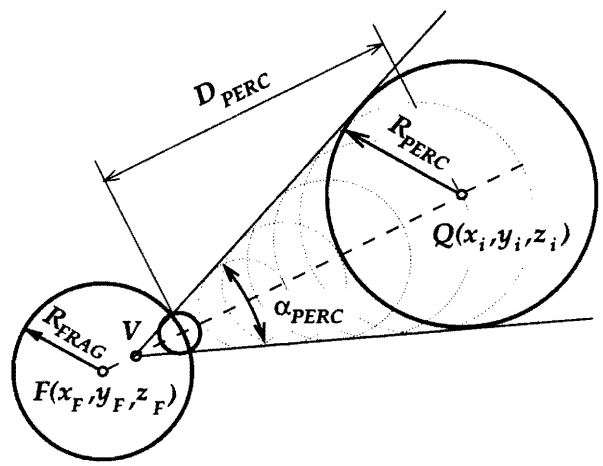

FIG. 4. Schematic two-dimensional presentation of the percolation sphere of radius R_{PERC} attributed to a free nucleon which moves along the axis (dashed line) of a percolation cone. The angle α_{PERC} gives the opening of the cone. Circle of radius R_{FRAG} represents the emitting heavy fragment whose center of gravity is at the point $F(x_F, y_F, z_F)$. The emitted nucleon, at the moment of emission, is lying on the heavy fragment surface and is represented by a small circle whose radius is equal to R^0_{PERC}. Its radial movement in time is represented by a set of growing dotted circles. At the moment when the percolation procedure is applied a nucleon has reached the point $Q(x_i, y_i, z_i)$. The position of the cone vertex V is given by the requirement that the cone should cut out, in the circle of radius R_{FRAG}, a chord of predefined length (the diameter of a bound nucleon) equal to $2 \cdot R^0_{PERC}$.

The above choice of the average speed $\bar{v}$ and, hence, of the constant α_{PERC} for all CS of the subensemble, is equivalent to the approximation that the sphere of radius R_{PERC}, i.e., each nucleon which is at the distance D_{PERC} from the heavy fragment, is seen from its source of emission (heavy fragment) under the same solid angle.

iii) Knowing α_{PERC} and D_{PERC}, the percolation radius R_{PERC} is calculated (see Eq. (7) below). A schematic two-dimensional illustration of quantities pertinent to the evaluation of R_{PERC} is shown in Fig. 4.

Having R_{PERC} defined for each nucleon, a percolation procedure is performed. Two nucleons are considered bound if they are closer to each other than the sum of their R_{PERC}, i.e., if their associated spheres overlap. Non physical clusters are rejected and broken into their basic constituents. Each cluster formed in a given event moves with the mean velocity of its constituents under the influence of the Coulomb repulsion of all other clusters. The calculation is stopped at 2000 fm/c when no further deviation of cluster trajectories occurs.

Our aggregation algorithm akin to a percolation approach, in fact, slightly differs from a standard one. Usually, when applying percolation methods in nuclear physics, nucleons are disposed on sites of a cubic lattice with either a given probability p for bounds between the sites to be effective (bound percolation [8,9]) or a given probability p that each available site is occupied by a nucleon (site percolation [37]). If one smoothly varies p, there is a critical value p_c such that for all $p > p_c$ an "infinite" cluster is formed traveling continuously throughout the lattice. This phenomenon is called *percolation* and represents a phase transition in the physical properties of the ensemble. Our probability of establishing links between nucleons is determined by the properties of the *phase space* driven by the LV dynamical calculation, i.e., by the topology of the configuration space and the subensemble mean speed $\bar{v}$ in momentum space, which determines neighborhood conditions to form light clusters. We have already stressed that we are dealing with regions of low average densities, and that their phase space distributions described in term of CS can be viewed as single particle emission probabilities [19]. Our CS represent the most classical single particle wave packets which expand after the emission following the quantum-mechanical spreading rate of a Gaussian wave packet. A free Gaussian wave packet with a spreading of $\Delta x(t_0)$ at the time t_o will spread, at the time $t = t_o + \Delta t$, to the value of [38]

$$\Delta x(t) = \sqrt{(\Delta x(t_0))^2 + (\hbar \Delta t / 2m \Delta x(t_0))^2}, \tag{4}$$

where m is nucleonic mass and $\hbar$ is the Planck constant. For the time intervals of interest here, the first term under the square root can be neglected, so that the expression (4) reads

$$\Delta x(t) \approx \hbar \Delta t / 2m \Delta x(t_0). \tag{5}$$

Here Δt is in fm/c and Δx is in fm. In other words, for sufficiently long times, the wave packet is spreading linearly with time, or, equivalently, with the distance it traveled. Since the packet is free, let v be the constant group speed of the wave packet. In a given time interval Δt the wave packet passes a distance $\Delta D = v \cdot \Delta t$. Using the approximation (5), an enveloping cone of opening angle

$$\alpha = 2 \cdot \arctan \frac{\Delta x(t) - \Delta x(t_0)}{2 \cdot \Delta D} \tag{6}$$

can be associated with a free wave packet. The center of gravity of the wave packet moves along the cone axes what is schematically represented in Fig. 4 by expanding dotted circles. The cone associated with the expanding wave packet, i.e., its opening angle and the vertex position,

determines the parameters of the *percolation cone* of Fig. 4. There is a full correspondence between v and $\bar{v}$, $\Delta x(t_0)$ and R^0_{PERC}, $\Delta x(t)$ and R_{PERC}, D and D_{PERC}, and α and α_{PERC}, respectively. Thus,

$$R_{PERC} = D_{PERC} \cdot \tan \frac{\alpha_{PERC}}{2} + R^0_{PERC}. \tag{7}$$

As already discussed, D_{PERC} is different for each nucleon. α_{PERC} is the same for all nucleons (CS) of the same subensemble since the $\bar{v}$ is the same, and R^0_{PERC} is a constant.

III. RESULTS

In the present investigation, we report on the results of simulations performed for the ^{40}Ar + ^{27}Al system at an impact parameter of $b = 5$ fm and Argon energy of 65 MeV/nucleon. As shown in Fig. 1, such a semi-peripheral reaction provides a well defined QP and QT. The LV code was run with the momentum-dependent nuclear interaction G1-D1 due to Gogny [26] and by taking $N_g = 100$. The random sampling procedure, explained in the previous section, was carried out on the initial population of $A \times N_g = 6700$ CS, and allowed to come down to a system of $A = 67$ nucleons. First of all, we verified that, due to sampling procedure, the total energy, the linear momentum and the angular momentum of the entrance channel are conserved in average. As one sees from Table 1, a good coherence between mean values of the constants of motion, for the total distribution of CS and for the generated percolation events, is obtained.

Also, we checked that the kinematic characteristics of the QP and QT have reasonable average values. Table 2 shows that the mean QP and QT values of mass, charge, polar angle and laboratory velocity, are very close for the generated percolation events and for the total population of CS, respectively.

In the following, we report the predictions of our clusterization model and make the comparison with the available experimental results for the Ar + Al system which has been recently extensively studied [39–43]. A number of theoretical investigations [20,44–47] have already been compared with these data. We will refer only to the most recent one [47]. To allow meaningful comparisons with experimental data and to illustrate the magnitude of instrumental distortions, we will show, both, unfiltered and filtered calculations. In the figures, the unfiltered theoretical results are depicted by hollow histograms whereas the filtered ones are hatched. The calculated observables presented in the figures are all extracted from 50 000 generated events.

Top of Fig. 5 shows the calculated charge distributions of the produced fragments. It is a typical distribution characterized by a steep decrease at low Z's followed by a plateau and, then, a second abrupt fall-off expressing a limit of the largest reaction Z value. For the same observable,

Table 1: Constants of motion for the Ar + Al reaction at 65 MeV/nucleon and $b = 5$ fm.

	Energy (MeV/nucleon)	Linear momentum (MeV/c/nucleon)	C.m. angular momentum ($\hbar$)
Entrance-channel value	65.0	207.7	140.1
Mean value per event	63.9	208.4	141.1

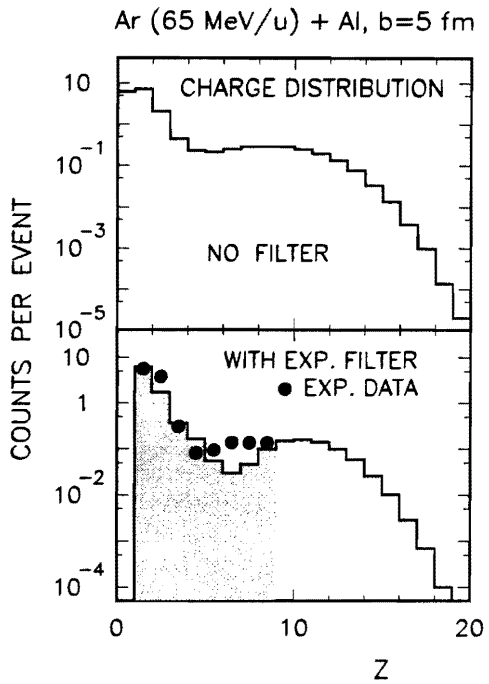

FIG. 5. The calculated charge distributions extracted from 50 000 events generated via simulation of the Ar + Al collision at 65 MeV/nucleon and an impact parameter of $b = 5$ fm. The upper panel displays the unfiltered and the lower one the filtered distributions. The latter one is obtained by filtering the generated events through the acceptance of the experimental device (geometry and thresholds). The points refer to the experimental values. The zone of the reliable experimental charge identification is hatched in the histogram.

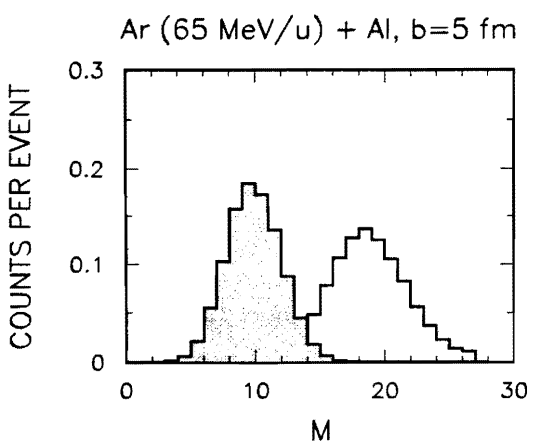

FIG. 6. The calculated event multiplicity. The unfiltered distribution is presented by hollow histogram and the filtered one by the hatched histogram. See, also, caption to Fig. 5.

bottom of Fig. 5 displays filtered calculations together with the experimental data [48]. As one can see from the figure, the main features of the data are well reproduced by the model calculations.

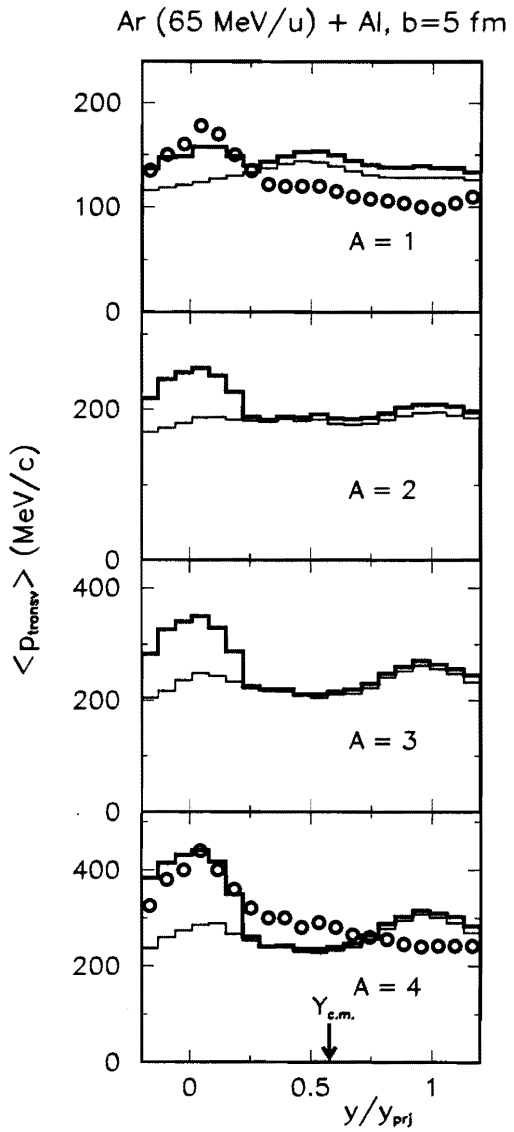

FIG. 7. From top to bottom, the calculated average transverse momentum per particle of $A=1$ to 4 species, respectively, as a function of relative rapidity. The thin line depicts distributions for which no filter was applied, whereas the thick one depicts filtered distributions. At the top and the bottom panel the experimental data are shown by open circles for $Z = 1$ and 2 particles, respectively. See, also, captions to Figs. 3 and 5.

Table 2: Quasiprojectile and quasitarget characteristics of the input phase space at the end of the LV dynamics and mean values of percolated events for the Ar + Al reaction at 65 MeV/nucleon and $b = 5$ fm.

	Quasiprojectile			
	Mass (u)	Charge	Angle (deg)	Velocity (cm/ns)
Entrance-channel value	22.3	9.8	-2.7	10.7
Mean value per event	23.3	10.9	-3.4	10.8
	Quasitarget			
	Mass (u)	Charge	Angle (deg)	Velocity (cm/ns)
Entrance-channel value	14.1	6.5	43.0	0.9
Mean value per event	14.5	7.2	44.0	1.6

Figure 6 displays the calculated multiplicity. Mainly due to undetected neutrons, filtered multiplicity is strongly shifted towards lower values. The mean value of this distribution is equal to 9 and is consistent with the experimental one which is located between 8.0 and 8.6 depending on the method used for determination of the experimental impact parameter [49].

From top to bottom, in Fig. 7 the average transverse momentum per particle $< p_{tr} >$, for particles with mass $A = 1$ to 4, respectively. are displayed. The mean value of $< p_{tr} >$ steadily increases with the particle mass but less than observed experimentally. For the $Z = 1$ and $Z = 2$ particles [43], the discrepancy is below 20 %. For the experimental $Z = 1$ particles the qualitative behavior of this observable is correctly reproduced by the simulation. However, the experimental $Z = 2$ distribution is not satisfactorily reproduced. The calculation underestimates average transverse momenta at mid- and overestimates them at projectile rapidity.

The hollow histograms in the right column of Fig. 8 show the unfiltered calculated relative rapidity distributions dN/dY_{rel} of different charge bins: light charged particles ($Z = 1$ and $Z = 2$) and intermediate mass fragments ($3 \leq Z \leq 5$ and $6 \leq Z \leq 9$), respectively. Three components are clearly present in these spectra: a projectilelike one, located near the projectile rapidity, a targetlike one, located near target rapidity, and the one in between, centered around the center-of-mass rapidity. This last component, very large for $Z = 1$ distribution, progressively disappears when the charge of considered fragments increases, vanishing for the last bin, $Z = 6$ - 9. These results can be compared with the recent calculations of Ono and Horiuchi [47] obtained with the AMD model [50]. The main difference between our results and those of Ref. [47] concerns this mid-rapidity component. In AMD calculations, the mid-rapidity component is present only in the distribution of nucleons and disappears for all kinds of clusters, particularly, for α particles [47].

From the filtered distributions (Fig. 8, hatched histograms), two features emerge. Firstly, the detection threshold increasingly suppresses the targetlike component of the distribution as the charge of clusters increases. Secondly, the mid- and projectilelike contributions are very little altered by experimental device, allowing to perform a reliable analysis of the characteristics of the intermediate and projectile sources. Let us now compare the filtered distributions with the experimental ones [43] (left column of Fig. 8). The overall features of the distributions, i.e., the relative contributions at mid- and projectile rapidities are correctly reproduced for each selected

charge bin. More quantitatively, the peak position of the projectile component for each charge bin is very close to the experimental one. Moreover, the integrals of these spectra are similar, within 10–15 %. However, for the $Z=2$ clusters, our model predicts twice less abundant production than observed in the experiment. This is not unexpected. In fact, α particles are largely dominating the measured $Z=2$ distribution. Obviously, using a crude topological prescription, one cannot hope to reproduce a particularly high probability for an α particle to be emitted in a nuclear reaction. This is due to a high stability of α particles, a phenomenon of a purely quantal nature.

Figure 9 shows the rapidity dependence of the calculated average in-plane transverse momentum $< p_x/A >$, A being the mass of the considered cluster. In the left column of the figure $< p_x/A >$ distributions for the species $A=1$ to 4, respectively, are plotted. The negative slopes of the momentum distributions near the center-of-mass rapidity indicate that the attractive nuclear

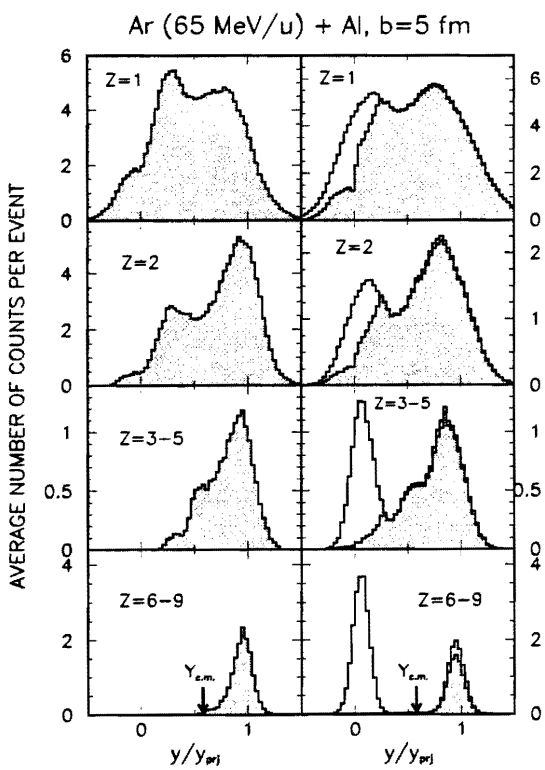

FIG. 8. From top to bottom, the relative rapidity distributions dN/dY_{rel} for particles in charge bins $Z = 1, 2, 3-5$ and $6-9$, respectively. The left column shows experimental distributions at an estimated impact parameter of $b \approx 4.5$ fm and the right one is the result of simulation for $b = 5$ fm with 50 000 generated events, respectively. On the right side, the filtered events are presented by hatched histograms, whereas the unfiltered distributions are presented by hollow histograms. Note the different scales used for the $Z=2$ panels on the left and the right column. See, also, captions to Figs. 3 and 5.

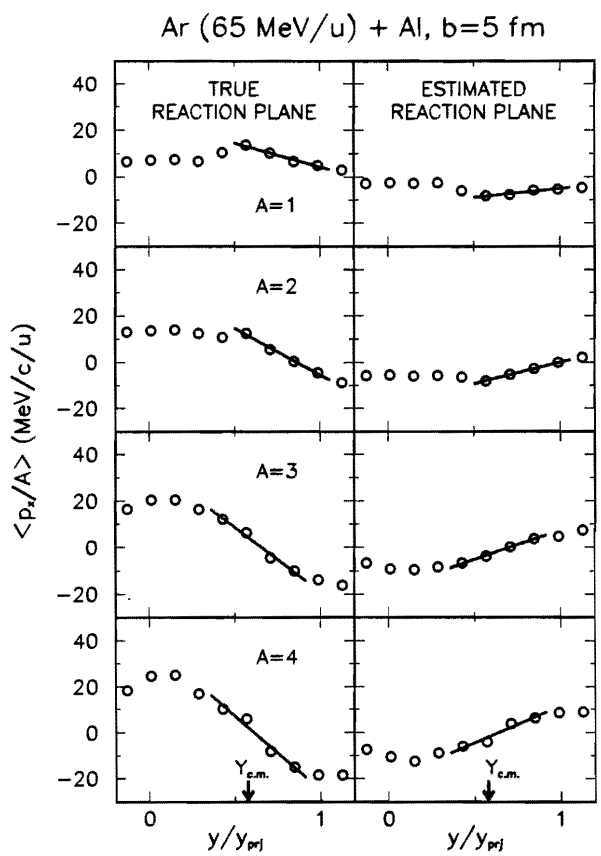

FIG. 9. From top to bottom, the calculated average value per nucleon, of the projection onto the reaction plane, of transverse momentum for $A = 1$ to 4 species, respectively, as a function of relative rapidity. The left column shows the results for a true reaction plane, whereas the right one shows the results obtained following the reaction plane determination as in [52]. The same procedure was used in the analysis of the experimental data [39,43]. See, also, captions to Figs. 3 and 5.

Table 3: Average transversal collective flow parameter (MeV/c/nucleon) defined by Eq. (8) for $A=1$ to 4 species emerging from the Ar + Al reaction at 65 MeV/nucleon and $b=5$ fm.

Charge or mass of clusters	This work b)	This work c)	Experiment[a)] Ref. [39]	Experiment[a)] Ref. [43]
$A=1$	-10.3 ± 2.1	3.9 ± 1.8	13 ± 2	8.5 ± 1.2
$A=2$	-20.1 ± 2.1	9.3 ± 1.8		
$A=3$	-27.6 ± 1.8	12.7 ± 1.4		
$A=4$	-32.2 ± 1.8	16.1 ± 1.4	28 ± 3	17.2 ± 1.7

a) Reported are values for $Z=1$ and 2 particles. No correction [53,54] for the systematic error in the reaction-plane determination was applied to the data.

b) The true reaction plane was used.

c) The reaction plane was determined using the transverse momentum method [52].

mean field dominates the interaction. At intermediate energies, the transversal collective flow is usually quantified by the mid-rapidity slope of the average transverse momentum per particle projected onto the reaction plane [51]:

$$\mathcal{F} = \frac{y_{prj} - y_{trg}}{2} \cdot \left. \frac{d < p_x/A >}{dy} \right|_{y=(y_{prj}-y_{trg})/2}, \tag{8}$$

where y_{prj} and y_{trg} are the projectile and the target rapidities, respectively. Consequently, the flow is extracted by linear fit of the $< p_x/A >$ distribution about the mid-rapidity. Expressed by the relative rapidity, $Y_{rel} = y_i/y_{prj}$, where y_i is the particle rapidity, Eq. (7) reads

$$\mathcal{F} = \frac{1}{2} \cdot \left. \frac{d < p_x/A >}{dY_{rel}} \right|_{Y_{rel}=0.5}. \tag{9}$$

The thick solid line drawn on each panel of Fig. 9, is the result of the fit to the data points. The extracted values of the parameter $\mathcal{F}$ are given in the second column of Table 3. As expected, the flow increases with the particle mass.

To make a reliable comparison with experiment, the events generated in the simulation must be treated in the same way as the experimental ones. From the experimental data [39,42,43], the flow was extracted using the transverse momentum technique of Danielewicz and Odyniec [52] in which estimation of the reaction plane and projection onto it, is carried out separately for each particle in a given event [52]. By applying this method to the calculation, the actual information on the reaction plane, known in the simulation, is forgotten. Since application of the detector acceptance does not alter the mid- and projectile rapidity regions (cf. in Fig. 8), the experimental filter is not taken into account for this study. Moreover, determination of the reaction plane is more sensitive to the method itself than to the detector acceptance. The right column of Fig. 9 displays deduced $< p_x/A >$ distributions and extracted values of the parameter $\mathcal{F}$ are given in the third column of Table 3. Let us make a few comments. Due to the unknown orientation of the estimated reaction plane, only absolute value of sidewards flow is obtained. Again, the absolute value of the flow increases with the mass of the particle. The projection of the transverse

momentum reaches its maximal value when projected onto the true reaction plane. Because of the reaction plane indetermination, the deduced values of the flow are smaller than those obtained with the true reaction plane.

To restore the actual value of the flow from the informations available in an experiment, two methods have been proposed [52–54]. These methods estimate the error involved in the determination of the reaction plane and give a corrective factor (CF) by which the experimental flow should be multiplied to get the "true" value of the sidewards flow. Since the true reaction plane is known in the simulation, we derive a CF by dividing the true and the estimated values of $\mathcal{F}$ resulting from our calculations. For all values of A the CF is nearly equal to 2, except for $A = 1$ for which the CF is 2.6. These values are consistent with experimentally deduced CF which varies between 1.5 and 2 [43] following both the used impact parameter sorting technique [43,55] and the adopted CF methods [52–54].

In last two columns of Table 3 the experimental values of the parameter $\mathcal{F}$ extracted from Refs. [39] and [43], are given. In these experiments, particles labeled $Z = 1$ and $Z = 2$ are largely dominated by protons and α particles, respectively. The estimated flow parameters for these particles agree well with those calculated for $A = 1$ and $A = 4$ species, respectively.

IV. SUMMARY

In this paper, we have shown that nuclear fragment formation below 100 MeV/nucleon can be successfully predicted using an original clustering approach. In contrast to the high energy regime, where a clear freeze-out time can be determined, below 100 MeV/nucleon the dynamical situation is much more complex and includes different emission processes which prevent a crude coupling of a dynamical and a geometrical approach. To overcome these problems, we had developed a clustering procedure based on a time dependent treatment of cluster formation. Our model, in a time-dependent way, creates clusters in the phase space provisioned by a semiclassical dynamical calculation with the Landau-Vlasov (LV) equation [17,26]. The main ingredients of our aggregation algorithm are as follows:

i) The *basic radius of percolation* R^0_{PERC}, whose value is imposed by the range of nuclear interaction, determines the wave-packet extension at the moment of emission.

ii) The *angle of percolation* α_{PERC} is determined by the average speed $\bar{v}$ of coherent states (CS) belonging to the given subensemble of free CS. It governs the rate of the wave packet extension, i.e., the actual value of R_{PERC}, as a consequence of the Gaussian form of CS.

iii) The *heavy fragment radius* R_{FRAG}, which is also given by the LV dynamics, defines source(s) from which the wave packets are emitted.

iv) The way how the ensemble of free CS of the LV phase space is decomposed into subensembles, i.e., the choice of a *set of consecutive times* to cut the emission process. This choice is essentially conditioned by the dynamics, in particular, the out-of-equilibrium phase and by sufficient statistics in each subensemble.

Obviously, there is not much freedom left to the adopted algorithm for cluster formation since the above constraints on the model parameters are mostly fixed by the LV dynamics used as an input for the generation of collision events.

Our parameter-free clusterization model has been applied to the Ar(65 MeV/nucleon) + Al reaction at $b = 5$ fm in order to compare its predictions with the experimental results. Our model

is able to reproduce quite well the Z-distributions, as well as the multiplicity and rapidity distributions. The evolution of the $< p_{tr} >$ and $< p_x/A >$ with the mass is also correctly reproduced but some discrepancies remain, especially, for α particles. These discrepancies stem from the following reasons. From an experimental point of view, the mixing of impact parameters, the recoil effects and the bias related to the experimental filter such as double counting are not taken into account in the simulation. From the theoretical side, rough phenomenological accounting for the nuclear interaction and multiparticle correlations in light clusters have to be settled and deserve more precise investigations.

ACKNOWLEDGMENTS

It is a pleasure to thank our colleagues from LPC Caen, in particular J.C. Angélique, G. Bizard, and J. Péter, for making their experimental results available to us before publication, and J.C. Steckmeyer for supplying us with the computer routine that simulates the response of the MUR-TONNEAU detector at GANIL. The authors appreciate M. Korolija from IRB Zagreb for the critical reading of the manuscript and a number of valuable comments. One of us (Z.B.) would like to express his gratitude to the *Laboratoire de Physique Subatomique et des Technologies Associées (SUBATECH)* for the warm hospitality during his stay as well as to the French Government for financial support.

References

[1] W.A. Friedman. *Ann. Phys. (NY)*, 192:146, 1989.

[2] J. Randrup and S.E. Koonin. *Nucl. Phys.*, A356:223, 1981.

[3] G. Fai and J. Randrup. *Nucl. Phys.*, A404:551, 1983.

[4] J.P. Bondorf, R. Donangelo, H. Schulz, and K. Sneppen. *Phys. Lett. B*, 162:30, 1985.

[5] D.H. Gross. *Nucl. Phys.*, A488:217c, 1988.

[6] D. Hahn and H. Stöcker. *Nucl. Phys.*, A476:718, 1988.

[7] D. Durand. *Nucl. Phys.*, A541:266, 1992.

[8] W. Bauer, D.R. Dean, U. Mosel, and U. Post. *Proc. Seventh High Energy Heavy Ion Study* (GSI Darmstadt, 1984), GSI Report-85-10, p. 701.

[9] X. Campi and J. Desbois. *Proc. Seventh High Energy Heavy Ion Study* (GSI Darmstadt, 1984), GSI Report-85-10, p. 707.

[10] T.S. Biro, J. Knoll, and J. Richert. *Nucl. Phys.*, A459:692, 1986.

[11] J. Desbois. *Nucl. Phys.*, A466:724, 1987.

[12] W. Bauer. *Phys. Rev. C*, 38:1297, 1988.

[13] H.R. Jaqaman, G. Papp, and D.H.E. Gross. *Nucl. Phys.*, A514:327, 1990.

[14] S. Leray, C. Ngô, M.E. Spina, B. Remaud, and F. Sébille. *Nucl. Phys.*, A511:414, 1990.

[15] L. Phair et al. *Phys. Lett. B*, 285:10, 1992.

[16] J.B. Garcia and C. Cerruti. *Nucl. Phys.*, A578:597, 1994.

[17] C. Grégoire, B. Remaud, F. Sébille, L. Vinet, and Y. Raffray. *Nucl. Phys.*, A465:317, 1987.

[18] E. Suraud, M. Pi, P. Schuck, B. Remaud, F. Sébille, C. Grégoire, and F. Saint-Laurent. *Phys. Lett. B*, 229:359, 1989.

[19] D. Ardouin, Z. Basrak, P. Schuck, et al. *Nucl. Phys.*, A514:564, 1990.

[20] V. de la Mota, F. Sébille, M. Farine, B. Remaud, and P. Schuck. *Phys. Rev. C*, 46:677, 1992.

[21] K. Sneppen and L. Vinet. *Nucl. Phys.*, A480:342, 1988.

[22] G. Montarou et al. *Phys. Rev. C*, 47:2764, 1993.

[23] F. Sébille et al. to be published.

[24] G.F. Bertsch and S. Das Gupta. *Phys. Rep.*, 160:189, 1988.

[25] J. Dechargé and D. Gogny. *Phys. Rev. C*, 21:1568, 1980.

[26] F. Sébille, G. Royer, C. Grégoire, B. Remaud, and P. Schuck. *Nucl. Phys.*, A501:137, 1989.

[27] E.A. Uehling and G.E. Uhlenbeck. *Phys. Rev.*, 43:552, 1933.

[28] B. Borderie et al. *Phys. Lett. B*, 205:26, 1988.

[29] J.C. Steckmeyer et al. Contrib. to the XXXIII Int. Winter Meeting on Nucl. Phys., Bormio (Italy), 1995.

[30] M.F. Rivet et al. *Phys. Lett. B*, 215:55, 1988.

[31] D. Jouan et al. *Z. Phys. A*, 340:63, 1991.

[32] A. Kerambrun et al. Preprint LPCC 94–14, Caen, 1994.

[33] P. Eudes et al. to be published.

[34] P. Abgrall, F. Haddad, V. de la Mota, and F. Sébille. *Phys. Rev. C*, 49:1040, 1994.

[35] J.R. Klauder and Bo-Sture Stagerstam. *Coherent states, application in physics and mathematical physics.* World Scientific, Singapore, 1985.

[36] X. Campi and J. Desbois. *Contrib. to the XXIII Int. Winter Meeting on Nucl. Phys.*, Bormio (Italy), 1985, 497.

[37] S. Das Gupta, C. Gale, and K. Haglin. *Phys. Lett. B*, 302:372, 1993.

[38] L.I. Schiff. *Quantum mechanics.* McGraw-Hill, New York, 1955.

[39] J.P. Sullivan et al. *Phys. Lett. B*, 249:8, 1990.

[40] D. Cussol et al. *Nucl. Phys.*, A561:298, 1993.

[41] W.Q. Shen et al. *Nucl. Phys.*, A551:333, 1993.

[42] J.C. Angélique et al. Contrib. to the XXXI Int. Winter Meeting on Nucl. Phys., Bormio (Italy), 1993.

[43] J.C. Angélique. Ph.D. Thesis, Univ. of Caen, 1993.

[44] H.M. Xu. *Phys. Rev. Lett.*, 67:2769, 1991.

[45] A. Ohnishi, T. Maruyama, and H. Horiuchi. *Comm. at Nucleus–Nucleus Collisions IV,* Kanazawa (Japan), 1991.

[46] Y. Ma, W. Shen, J. Feng, and Y. Ma. *Z. Phys. A*, 344:469, 1993.

[47] A. Ono and H. Horiuchi. *Phys. Rev. C*, 51:299, 1995.

[48] J.-C. Angélique and J. Péter. Private communication and to be published.

[49] J.C. Angélique. Private communication.

[50] A. Ono, H. Horiuchi, T. Maruyama, and A. Ohnishi. *Prog. Theor. Phys.*, 87:1185, 1992.

[51] J.P. Sullivan and J. Péter. *Nucl. Phys.*, A540:275, 1992.

[52] P. Danielewicz and G. Odyniec. *Phys. Lett. B*, 157:146, 1985.

[53] P. Danielewicz and G. Odyniec. *Phys. Rev. C*, 38:120, 1988.

[54] M. Demoulins. Ph.D. Thesis, Univ. of Paris-Sud, 1989.

[55] J. Péter et al. *Nucl. Phys.*, A519:611, 1990.